Engineering Fracture Mechanics Vol. 17, No. 4, pp. 367–379, 1983
Printed in Great Britain.

0013-7944/83/040367-13$03.00/0
Pergamon Press Ltd.

RAIN EROSION DAMAGE IN BRITTLE MATERIALS

S. VAN DER ZWAAG† and J. E. FIELD
Cavendish Laboratory, Madingley Road, Cambridge, England

Abstract—In order to understand the processes involved in the high-velocity rain erosion of brittle materials the impact damage produced in soda-lime-silica glass by single and multiple jet impact was studied. The damage was quantified by measuring the post-impact strength of specimens. It is shown that the impact damage depends on the impact velocity, the number of impacts and the specimen dimensions. A new analysis for calculating the velocity dependence of jet/drop impact damage in brittle materials is presented. The model is based on Hertzian contact analysis and dynamic fracture mechanics and takes into account the statistical nature of the flaws in the specimen. A good qualitative agreement with experimental results is obtained.

1. INTRODUCTION

FORWARD-facing aircraft components may suffer damage due to the impact with rain drops. This damage may take the form of paint stripping, pitting of aerofoils and failure of rivets (see [1]). However, rain erosion is a more serious problem for brittle components, such as glass or plastic domes and covers and fibre reinforced plastic or ceramic radomes, where multiple drop impacts may result in catastrophic failure. In the case of brittle materials the impact damage is primarily due to the interaction of the Rayleigh surface wave, which is generated during the impact, with pre-existing surface defects such as flaws and scratches [2, 3]. Such an interaction may lead to crack growth and subsequent material removal and strength reduction.

In the drop impact process two regimes can be distinguished. Firstly an initial stage during which very high pressures are generated due to the compressible behaviour of the liquid [4]. It continues as long as the contact area between the impacting drop and the solid expands supersonically with respect to the waves in the liquid [2, 5–7]. The duration of this stage depends on the impact velocity and the radius of curvature of the drop but is generally in the range of 0.1–1 μs. In the second stage of the impact the shock waves generated by the impact move up the free surface of the drop, jetting begins and the impact pressure drops to lower values due to incompressible flow. For a 500 m s^{-1} impact the incompressible flow pressure is only about 10% of the pressures generated in the compressible regime. Most of the impact damage in brittle materials is associated with the initial high-pressure regime. It is for this reason that liquid jets with a smoothly curved front profile can be used to simulate drop impact.

In the present work the impact damage in brittle materials is examined as a function of the impact velocity, the number of impacts and the specimen size, using the jet technique originally developed by Bowden and Brunton [8]. The jet technique, in which jets are fired at stationary specimens, has great operational advantages over a more realistic but very complicated experiment of a stationary drop and a moving specimen. The impact damage has been quantified by measuring the post-impact strength of the specimens. Soda-lime glass was used in the experiments because it has been and is extensively used as an aircraft window material and studies of its erosion behaviour are therefore of practical interest. Furthermore, in basic studies where a great number of specimens are required it has the advantage of availability and low cost. A theoretical model for calculating the jet/drop impact damage in brittle materials is presented. Good qualitative agreement with experimental results is obtained.

2. EXPERIMENTAL

The high-velocity (> 100 m s^{-1}) water jets used in this study were produced by a technique originally developed by Bowden and Brunton [8]. In this technique a lead slug is fired with a 0.22 calibre air-rifle into the rear of a water-filled stainless steel nozzle. The forward motion of the sealing neoprene disc extrudes the water at high velocity through the orifice section at the front of the nozzle.

A newly designed nozzle for 0.8 mm dia. jets has been used which gives very reproducible impact

†Present address: Department of Metallurgy, Technical University Delft, Delft, The Netherlands.

damage over a wide velocity regime [9]. Field *et al.* [10] have compared the dimensions of the impact damage on PMMA due to a single jet impact with those for single spherical drop impacts and have concluded that these 0.8 mm jets simulate the impact of ~4 mm dia. drops for the velocity range of 300–700 m s^{-1}. Although Cherry *et al.* [11] have shown that the maximum drop dia. in a rainfield can approach 9 mm, the largest raindrops commonly found are 2–3 mm in dia. [12]. The jets used here simulate therefore relatively large but rare raindrops. However, the contribution of these few large drops to the overall rain erosion damage can be significant since the impact damage increases rapidly with the drop size, or more precisely the local radius of curvature at the point of first contact.

The soda-lime-silica glass specimens were in the form of discs with a radius of 25 mm and an average thickness of 2.98 mm. The specimens were impacted in the as-received condition. The impacts were performed such that all the impacts were at the centre of the specimen. By this arrangement the cumulative effect of multipole jet impact was as large as possible. Specimens were not dried between successive shots since the amount of water adhering to the surface was small. Furthermore, the "undried" surface approaches the in-flight conditions better. At least 15 specimens were used for each impact condition. The specimens were held rigidly around their circumference during impact.

The hydraulic bursting technique described earlier [13, 14] was used to measure the fracture stress of specimens after liquid jet impact and to quantify the impact damage.

In some experiments the specimens were fully supported by, and acoustically matched to, a 25 mm thick glass disc. By comparing the impact damage for the two support conditions the effect of stress wave reflections and bending stresses on the impact damage could be determined.

3. RESULTS

The various ways in which the data obtained can be analysed [15] are first discussed in detail for the case of single impact. The introduced concepts are then used to clarify the "residual strength" curves obtained for multiple impact.

3.1 *Single liquid jet impact*

Specimens were subjected to single normal jet impacts in the velocity range 125–700 m s^{-1}. Typical impact damage patterns are shown in Fig. 1 for three impact velocities. The damage consists of a central undamaged zone surrounded by short circumferential cracks. The density and average size of these cracks increases with increasing impact velocity. At low impact velocities no impact damage could be detected. The average fracture stresses of the specimens after impact are plotted as a function of the impact velocity in Fig. 2. This "residual strength" curve shows that a critical impact velocity has to be reached before a reduction in the average fracture stress is observed. This threshold velocity is followed by a transition region (150–300 m s^{-1}), in which the average fracture stress decreases rapidly with increasing impact velocity. At high impact velocities the average fracture stress is a much weaker function of the impact velocity.

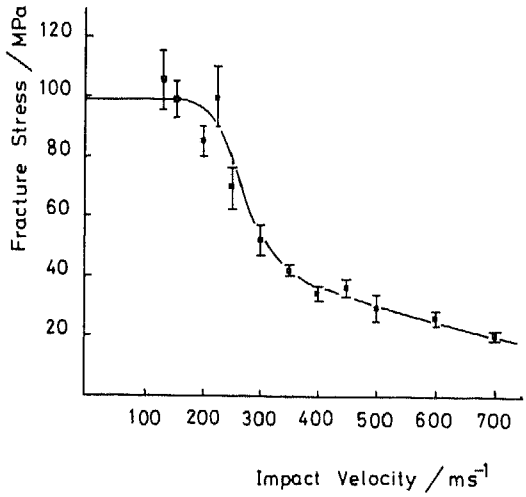

Fig. 2. Variation of the residual fracture stress with jet impact velocity for soda-lime glass. Jet from 0.8 mm orifice. Error bars indicate standard deviation of the mean.

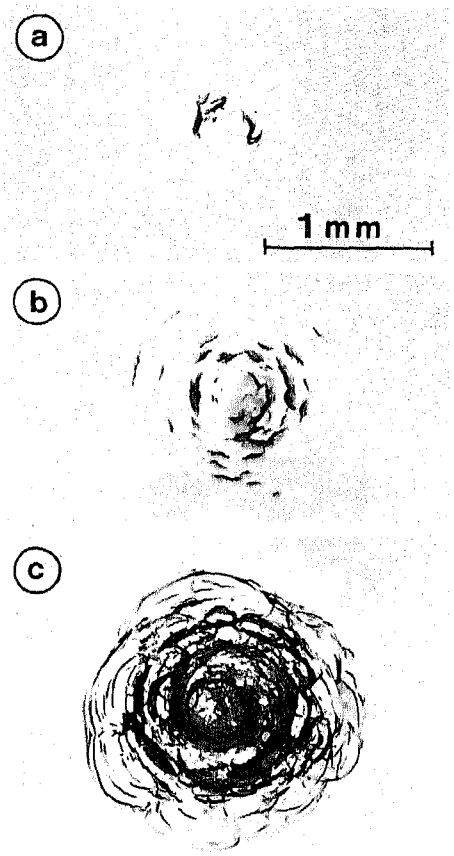

Fig. 1. Examples of impact damage in soda-lime glass due to jet impacts from a 0.4 mm nozzle. Equivalent to impacts with ~2 mm diameter drops. (a) 300 m s^{-1}, (b) 450 m s^{-1}, (c) 700 m s^{-1}.

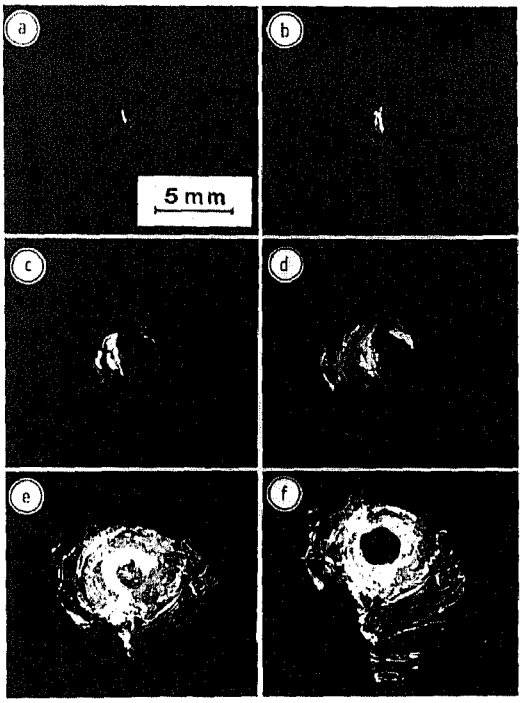

Fig. 7. Typical increase of jet impact damage with the number of impacts. Jet from 0.8 mm orifice. Impact velocity 250 m s^{-1}; (a) after 2 impacts; (b) after 3 impacts; (c) after 5 impacts; (d) after 8 impacts; (e) after 15 impacts; and (f) after 23 impacts.

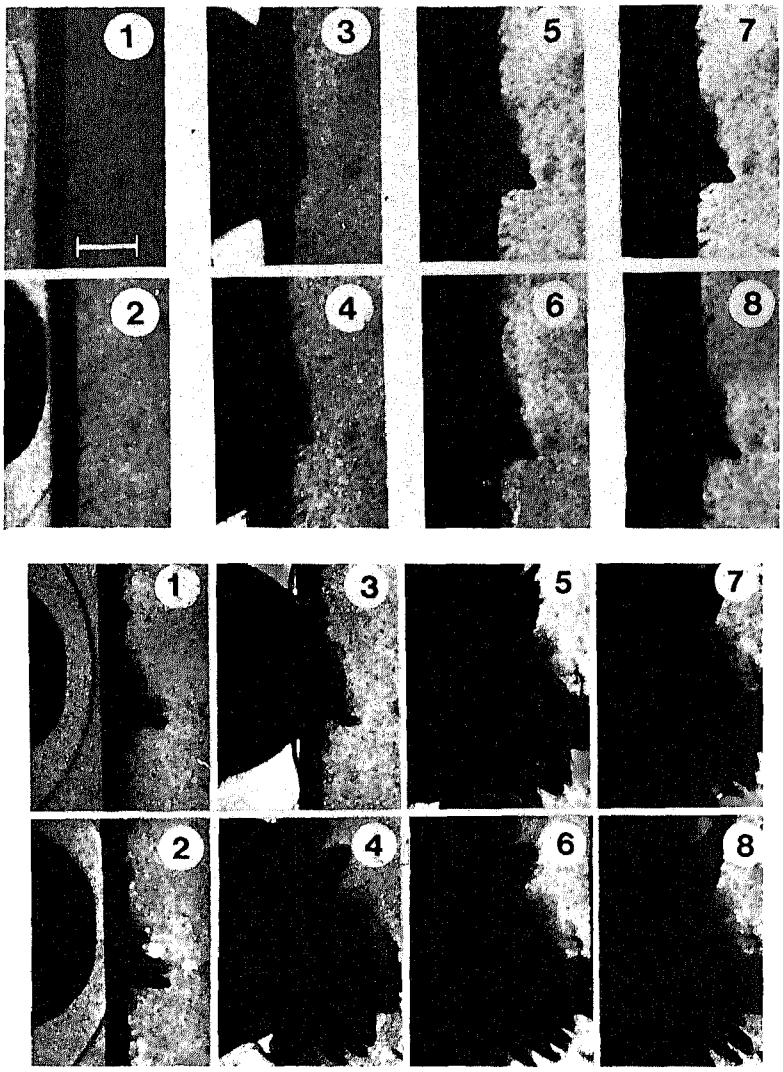

Fig. 11. Side view of a 0.8 mm jet impacting a glass specimen at 500 m s^{-1}. Time interval between frames 1 μs; (a) impact on as-received specimen; (b) a second impact on the specimen impacted in (a). Note the air shock travelling ahead of the jet.

In the transition region there is a bimodal distribution of fracture stresses. Some specimens have a low fracture stress, while others fail at a stress comparable to that for unimpacted specimens. The percentage of specimens with low fracture stress increases with impact velocity. At impact velocities above 400 m s^{-1} all specimens fail at a low fracture stress. To show this aspect more clearly the average fracture stresses for the two groups are plotted separately in Fig. 3. The data can also be expressed in terms of the probability that the fracture strength of the specimen is reduced by the impact. The probability curve for single impact is shown in Fig. 4.

It should be emphasized that earlier work by Rickerby[15] using high-speed photography has shown that the variability of the results in the transition region is not caused by jet instabilities but is due to variations in surface flaw distributions. This explanation is supported by a new theoretical analysis of the impact damage which is described later.

As pointed out by Matthewson and Field[14], the measured fracture stress can be used to calculated the size of the flaw leading to failure of the specimen. In general the equivalent flaw size, c, can be calculated from the fracture stress, σ_f, and the critical stress-intensity factor, K_{1c}, using

$$c = \alpha(K_{1c}/\sigma_f)^2 \tag{1}$$

where α is a dimensionless constant depending on the flaw and stress field geometry. In the present work the crack geometry is taken as semicircular. For this type of crack in a uniaxial bending stress field $\alpha = 0.75$[16]. Inserting in the above equation the appropriate values for the stress intensity factor ($K_{1c} = 0.75$ MNm$^{-3/2}$) and fracture stress ($\sigma_f = 100$ MPa), an average equivalent flaw size of about 42 μm

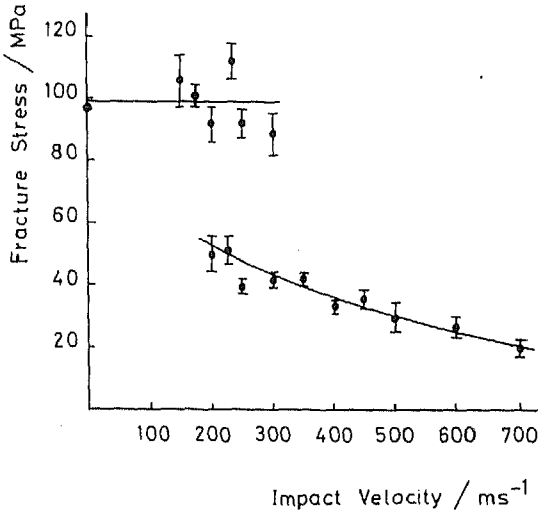

Fig. 3. Same data as in Fig. 2 but now results for "undamaged" and damaged specimens plotted separately.

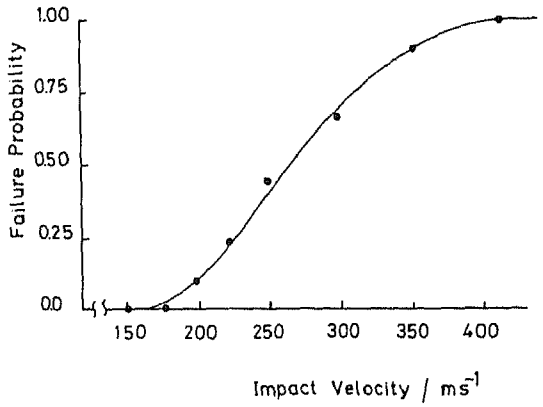

Fig. 4. Variation of failure probability with jet impact velocity. Same data as in Fig. 2. Estimated uncertainty ± 10%.

is calculated for unimpacted specimens. This value agrees quite well with the inherent flaw dimensions of 34 μm reported by Mecholski *et al.*[17]. The slightly larger value obtained here probably arises from slow crack growth during testing of the specimens in the pressure tester (test duration typically 30 sec.).

The calculated equivalent flaw sizes for impacted specimens have been plotted in Fig. 5 as a function of the impact velocity. A good agreement between calculated and observed flaw dimensions was obtained.

3.2 *Multiple liquid jet impact*

The residual strength curves for double, triple, 5-fold and 10-fold impact per specimen are shown in Fig. 6. In this figure the residual strength curve for single impact is also included. The most salient features of this figure are the decrease in average fracture stress with the number of impacts and the reduction in the width of the transition region. The onset of the transition region however remains essentially the same with only a very small decrease.

A typical example of the increase in impact damage with the number of impacts is shown in Fig. 7 for impacts at 250 m s^{-1}. Not only do cracks grow due to subsequent impacts but also new cracks become visible. The semi-apex angle of the conical envelope of the deeply penetrating cracks near the centre of

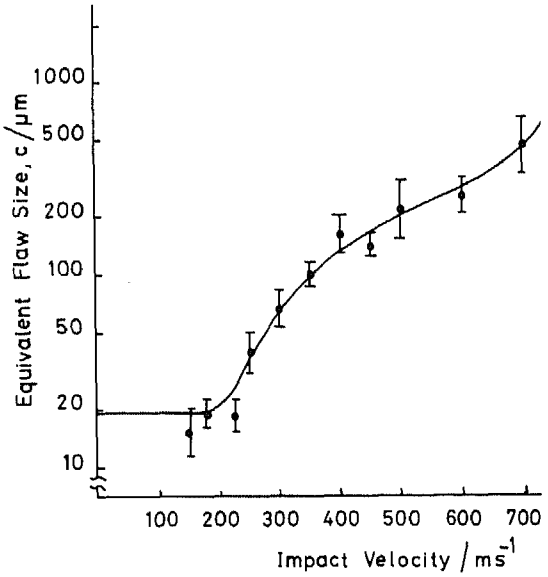

Fig. 5. Variation of equivalent flow size with jet impact velocity. Same data as in Fig. 2.

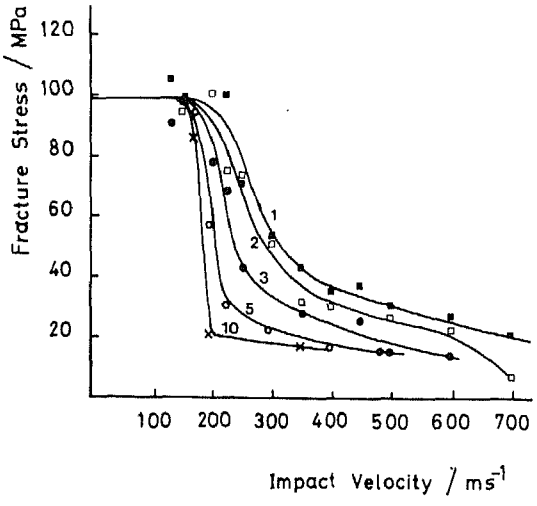

Fig. 6. Variation of residual fracture stress after single and multiple jet impact with impact velocity.

the impact is about 30° which is considerably smaller than for static loading (about 65°). A similar reduction in the cone angle has been reported for high speed solid sphere impacts on glass[18]. No suitable explanation for the loading-rate dependence of the cone angle is yet available. At high impact velocities or at a large number of impacts, the cone crack intersects the rear surface of the specimen and creates a hole in the centre of the specimen (Fig. 7f). This phenomenon, which is clearly dependent upon the specimen geometry, causes the plateau of minimum fracture stress at about 20 MPa in the residual strength curves.

The very low fracture stress obtained for double impact at 700 m s^{-1} is due to the formation of radial cracks, emanating from the centre of the rear surface. A combination of bending stresses and stress wave reflections provides the driving force for these cracks. Similar cracks are not observed under identical impact conditions on thick and large plates of glass.

To show more clearly the increase in impact damage with number of impacts, the fracture stresses of damaged specimens only are plotted in Fig. 8. No statistically significant change in the initial plateau region could be detected for multiple impacted specimens.

The failure probability curve, plotted in Fig. 9, shows that the velocity regime in which the fracture stress distribution is bimodal is significantly reduced. It should also be emphasized that the threshold velocity for impact damage seems to decrease only very slowly with increasing number of impacts.

The equivalent flaw sizes, calculated according to eqn (1), are plotted in Fig. 10 and are in good agreement with the observed crack dimensions. It is clear from this figure that the average crack growth during the second and subsequent impacts is larger than during the first impact. This is confirmed by *in situ* observations of the crack growth during impact using high speed photography as shown in Fig. 11. In Fig. 11(a) a side view of a jet impact at 500 m s^{-1} on an unimpacted glass block is presented. The

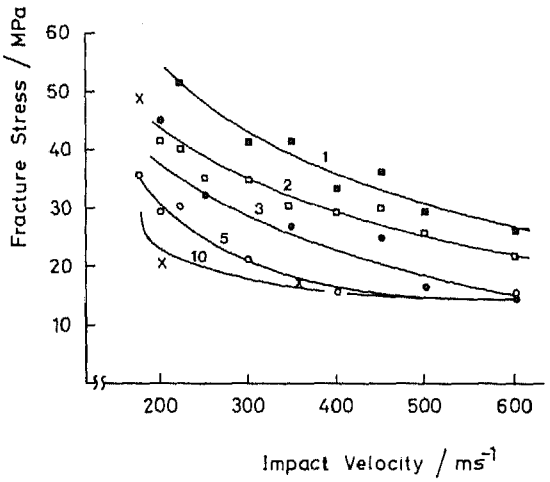

Fig. 8. Residual strength curves for single and multiple jet impacts. Results for damaged specimens only.

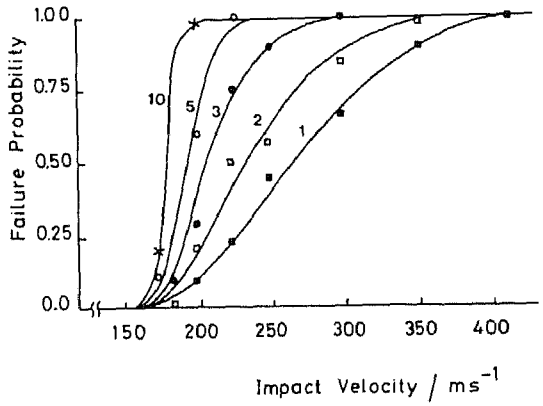

Fig. 9. Failure probability curves for single and multiple jet impacts.

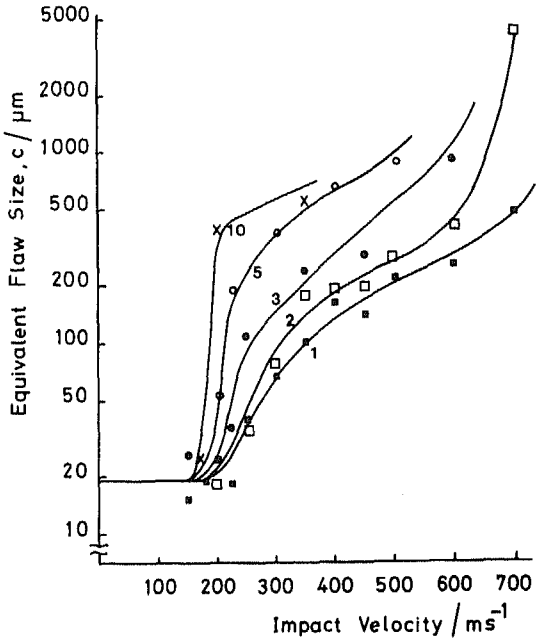

Fig. 10. Equivalent flaw size curves for single and multiple jet impacts.

cracks start to grow during the first micro second after impact and continue to grow for about 3 μs. When the specimen is impacted a second time under the same conditions both the average crack velocity and the time interval during which the crack grows increases.

3.3 *The effect of stress wave reflections*

In order to investigate the combined effect of bending stresses and stress wave reflections from the rear surface, single and double jet impact experiments were performed on specimens centrally supported by, and acoustically matched to a 25 mm thick glass plate. The residual strength curves are shown in Figs. 12 and 13 for single and double jet impact respectively. The figures show that bending stresses and stress wave reflections do indeed contribute to the impact damage. Their contribution is especially important for high velocity impacts. No effect could be detected for impact velocities just above the threshold velocity.

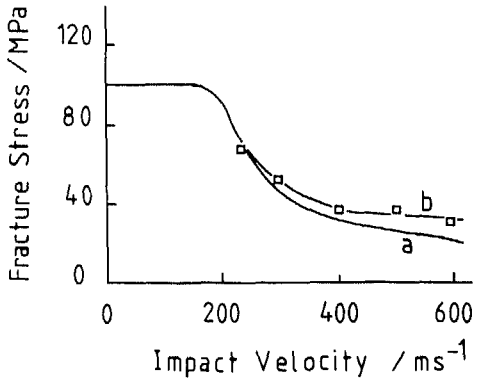

Fig. 12.

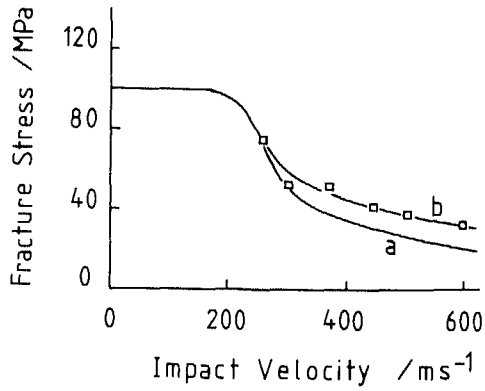

Fig. 13.

Fig. 12. Residual strength curves for 3 mm thick soda-lime glass specimens after single impact; (a) unsupported specimens; (b) supported specimens.

Fig. 13. As Fig. 12 but for double impact.

4. DISCUSSION

It has been shown that jet impact damage in brittle materials is in the form of small circumferential cracks around the impact site and that the size and the density of the cracks increases with the impact velocity. Earlier experiments by Field [2, 3] have shown that these cracks are due to the interaction between the Rayleigh wave and pre-existing surface defects. The observed velocity dependence of the impact damage can be explained qualitatively in terms of pulse intensity and flaw size distribution. At low impact velocities the stress wave intensity is too low to cause extension of any of the flaws present on the surface and the impact does not affect the flaw size distribution and hence the fracture stress of the specimen. At higher impact velocities the pulse intensity and pulse duration increase and for some of the defects, in particular the larger ones in the vicinity of the impact site, the critical conditions for crack growth are met and crack extension occurs. When the size of one of the extended defects becomes larger than the largest initial flaw the impact has resulted in a loss of strength. Since in this velocity regime the occurrence of impact damage depends critically on the size of the flaws close to the impact centre the inherent variability in flaw sizes and positions in brittle materials leads to a loss of strength for some specimens while others remain undamaged under the same impact conditions. At higher impact velocities the probability of "finding" a flaw of sufficient size in the vicinity of the impact increases until at high impact velocities all specimens show a loss of strength because of the impact.

Although the increase in damage with the number of impacts seems hardly surprising it should be mentioned that there is here a large difference between static and dynamic loading. In quasi-static loading with a rigid sphere the dimensions of the resulting cone crack are entirely determined by the material properties and the applied load. A reapplication of the same load, assuming no stress corrosion or interfacial frictional effects, does not extend the crack beyond its initial size. However, in the dynamic case the extent of the crack growth is not only determined by the magnitude of the stress pulse but also by its *duration* which limits its growth. Subsequent impacts effectively give further time for crack growth and the crack continues to develop until K_{1c} is no longer exceeded at the crack tip.

So far it has been assumed that the damage is only due to the Rayleigh wave. However, longitudinal waves reflected from the rear surface can enhance the Rayleigh wave and increase the crack growth. The position at which this reinforcement occurs depends on the relative velocities of the Rayleigh and longitudinal waves and the specimen thickness [2, 3]. This process only makes a significant contribution to the damage at high impact velocities and relatively thin specimens. It should be emphasized that glass has a low acoustic attenuation coefficient and many other materials will not be susceptible to these reinforcement effects until correspondingly higher velocities.

We now consider in more detail the various parameters and combine them to give a simple quantitative model for liquid impact damage in brittle materials.

Stress wave intensity

Swain and Hagan [19] have attempted to measure the magnitude and time dependence of the Rayleigh surface wave produced by an impacting jet using piezo-electric crystals. They were unable to determine the absolute magnitude of the pulse but showed that the Rayleigh wave can be approximated, to a reasonable accuracy, by a triangular pulse. As a first approximation they used the following expression for the amplitude of the Rayleigh wave

$$\sigma_{max} = \beta Z V_i \tag{2}$$

where β is a constant, Z the acoustic impedance of the liquid and V_i the impact velocity. The above equation was derived by drawing an analogy with the case of quasi-static Hertzian contact where the maximum radial tensile stress depends linearly on the average pressure over the contact zone.

Dynamic crack growth

In the case of a dynamically loaded crack the stress intensity factor is initially a function of time [20–22]. For a stationary crack the diffraction of the stress wave by a crack of finite dimensions leads to a damped oscillatory behaviour of the stress intensity factor around the quasi-static value.

The stress intensity factor for a non-stationary crack has been analysed in several studies [23–28]. The equation for the stress intensity factor derived by Eshelby [24] is particularly applicable to the

problem of propagating small flaws and is given by

$$K_{1d} = m\sigma(\pi a)^{1/2}(1 - V/C_R)^{1/2}U \tag{3}$$

where m is a geometrical constant, a the initial flaw size, V the current crack velocity, C_R the Rayleigh wave velocity and U is given by the following series

$$U = \left[1 + \frac{3}{8}\frac{c-a}{a} - \frac{15}{256}\left(\frac{c-a}{a}\right)^2 + \ldots.\right] \tag{4}$$

where c is the current crack size. Evaluation of this series shows that for $c < 20a$ U can be accurately approximated [26] to

$$U \simeq \left(1 + \frac{4}{5}\frac{c-a}{a}\right)^{1/2} \tag{5}$$

The current crack velocity in the above equation can be derived from the experimentally determined dependence of the crack velocity on the dynamical stress-intensity factor [29]

$$V = V_{\max}(1 - K_{1c}^2/K_d^2) \tag{6}$$

where $V_{\max}$ is the maximum crack velocity.

Flaw statistics

The variability in the strength of nominally identical brittle specimens is due to a distribution in the size of the "Griffith" flaws. Hunt and McCartney [30] have derived an expression relating the failure probability to the flaw size distribution. A simplified probability density function for the flaw dimensions has been derived by Jaytilaka and Trustrum [31] from experimental data and is given by

$$f(c) = \frac{c_0^{n-1}}{(n-2)!}c^{-n}\,e^{-c_0/c} \tag{7}$$

where c_0 is the size of the most probable flaw dimension. The parameter n is related to the Weibull parameter m [32].

THE MODEL

In order to calculate the residual strength curve for soda-lime glass the following procedure has been followed:

(i) In a circular specimen flaw positions were generated at random. The total numbers of flaws per specimen was between 20 and 40.

(ii) A flaw dimension was allocated to each of the flaw positions. All flaws were taken as normal to the radial vector from the centre of the specimen. The flaw size distribution used in the calculations is

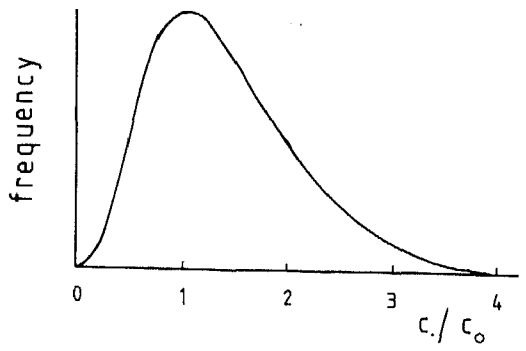

Fig. 14. Probability density function of flaw sizes which is used in the calculation of the residual strength curve for soda-lime glass.

plotted in Fig. 14. The most frequent crack dimension was taken as 12 μm; 99% of the flaws have dimensions smaller than 50 μm.

(iii) The maximum flaw size in the specimen was used to calculate the pre-impact strength of this specimen.

(iv) The impact was simulated by a stress pulse, i.e. the Rayleigh wave, moving radially outwards from the centre of the specimen. In order to simplify the calculations the stress pulse was taken as rectangular. The amplitude of this pulse decayed as $R^{-1/2}$, i.e. the same decay rate as the Rayleigh wave, when moving outwards over the specimen. The initial duration of the stress pulse was taken as 0.1 μ s. The duration of the pulse was increased linearly with radial distance.

(v) At each flaw position the dynamical stress intensity factor was calculated according to eqn (3). For flaws where K_{Id} exceeded K_{Ic} crack growth was calculated using an iteration procedure in which the stress pulse was divided in 100 intervals of equal duration. For each interval the current crack velocity was calculated using eqn (6). From this crack velocity the crack growth during the interval was calculated and added to the current crack dimension calculated in the previous interval. In the calculations the appropriate values for K_{Ic} (0.75 MNm$^{-3/2}$) and maximum crack velocity (1500 m s^{-1}) have been used.

(vi) From the maximum flaw size after impact the post-impact strength of this specimen was calculated. By comparing the pre- and post-impact strength of the specimen the occurence of impact damage could be determined.

(vii) The above procedure was repeated for a 100 specimens under identical impact conditions. For each impact velocity the average fracture stress and the probability that the fracture stress is reduced by the impact were calculated.

(viii) Finally the initial stress pulse amplitude, i.e. the impact velocity (eqn 2), was stepwise increased and the whole procedure was repeated for each pulse amplitude.

The results of the calculations have been plotted in the form of a residual strength curve in Fig. 15. A very good qualitative agreement with the residual strength curve for single impact is obtained. In particular the variation in the amount of scatter in the fracture stress as a function of the impact velocity is well reproduced in the analysis. From the analysis a failure probability curve can be obtained which is also shown in Fig. 15 (broken line). Once again a good qualitative agreement with the measured probability curve is obtained. The model has also been used to calculate the effect of multiple impacts on the resulting damage and the same conclusions as from the experimental results can be made, namely an almost constant threshold velocity, a reduction of the width of the transition region and a continuous increase in the post-impact flaw size at high impact velocities.

The model can also be used to illustrate the effect of abrasion on the residual strength curve. For this purpose a new set of specimens with twice the density of flaws was generated. Furthermore, the size of the most frequent defect was increased to 25 μm with 99% of the defects smaller than 100 μm. The impact parameters and material properties were not changed. The residual strength curves for the "as received" (open circles) and the "abraded" specimens (closed circles) are plotted in Fig. 16. Due to the

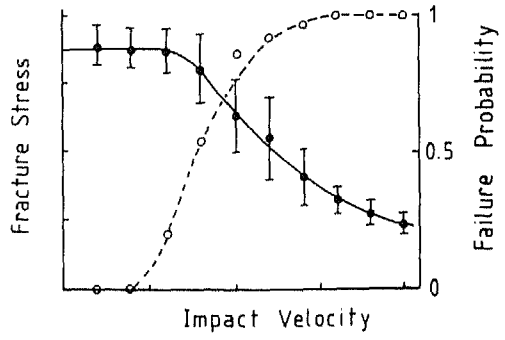

Fig. 15.

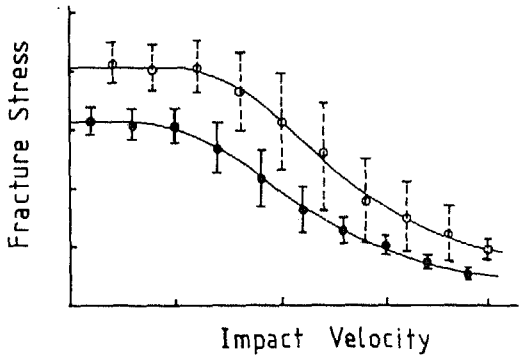

Fig. 16.

Fig. 15. Theoretical residual strength curve (——) and failure probability curve (----) for soda-lime glass (see text).

Fig. 16. Theoretical residual strength curves for soda-lime glass (see text). ○ "as received" specimens. ● "abraded" specimens.

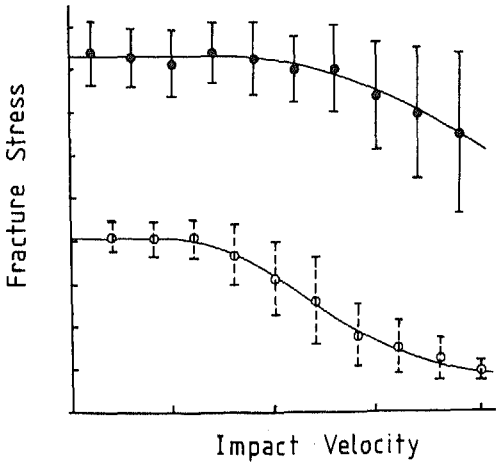

Fig. 17. Theoretical residual strength curves for soda-lime glass (O) and "tough material" (●).

abrasion not only the initial strength of the specimens is reduced but also the threshold velocity and the post impact strength at high impact velocities. The failure probability curve (not shown) shows a much smaller transition region for the "abraded" specimens. The above predictions are in very good agreement with experimental data for jet impact studies[33]. Furthermore, Wiederhorn and Lawn[34] noted similar effects for solid particle impacts on abraded and unabraded glass specimens.

Finally, in Fig. 17 the beneficial effect of increased toughness of the specimens is illustrated. The solid line indicates the residual strength curve for a material with $K_{1c} = 1.5$ MNm$^{-3/2}$ (twice that of the reference material). The other impact and material parameters are as for the reference condition. It should be mentioned that such an increase in impact resistance can also be obtained by polishing the specimens, i.e. producing smaller flaws with a lower density. However, in practice polishing is not a feasible technique for improving the rain erosion resistance because of the problems associated with maintaining the surface finish.

5. CONCLUSIONS

The present study has been concerned with liquid impact damage in brittle materials. It was found that there are three stages in the impact velocity—damage relation:

(i) At impact velocities below the threshold velocity the post impact stress is always comparable to that for unimpacted specimens. The threshold velocity depends only weakly on the number of impacts. Therefore, a meaningful estimate of the threshold velocity under practical conditions can be obtained from single impact experiments.

(ii) At high impact velocities all impacted specimens have a considerably reduced residual strength. The loss of strength increases with the number of impacts. The damage is in the form of short circumferential cracks around an undamaged central zone and resembles that due to Hertzian contact.

(iii) At intermediate velocities the results of the residual strength measurements show a bimodal distribution: some specimens have an "undamaged" fracture stress while others (impacted at the same velocity) fail at reduced stress levels. The ratio of undamaged/damaged specimens varies continuously over this transition region. The width of this region decreases rapidly with the number of impacts.

The velocity dependence of the damage in brittle materials can be explained on the basis of the interaction of the Rayleigh wave with surface defects and the ensuing extension thereof. The transition region is due to the statistical nature of the flaw distribution over the specimen surface. A model based on the above concepts shows good agreement with experimental results. Using this model the detrimental effects of large initial flaws and the beneficial effects of increased toughness on the rain erosion resistance have been illustrated.

Acknowledgements—The work was supported in part by the Ministry of Defence (Procurements Executive) and by the US Air Office of Scientific Research, Grant 783705. We thank Dr. M. J. Matthewson, Dr. J. T. Hagan, Dr. N. S. Corney and Professor D. Tabor for comments on the manuscript.

REFERENCES

[1] J. H. Brunton and M. C. Rochester, Erosion. *Treatise on Materials Science*, Vol. 16, (Edited by C. M. Preece). Academic Press, New York (1979).
[2] F. P. Bowden and J. E. Field, The brittle fracture of solids by liquid impact, by solid impact and by shock. *Proc. Roy. Soc. Lond.* **A282**, 331–352 (1964).
[3] J. E. Field, Stress waves, deformation and fracture caused by liquid impact. *Phil. Trans. Roy. Soc. Lond*, **A260**, 86–93 (1966).
[4] S. S. Cook, Erosion by waterhammer. *Proc. Roy. Soc. Lond.* **A119**, 481–488 (1928).
[5] F. J. Heymann, High-speed impact between a liquid drop and a solid surface. *J. Appl. Phys.* **40**, 5113–5122 (1969).
[6] J. E. Field, M. B. Lesser and P. N. H. Davies, Theoretical and experimental studies of two-dimensional liquid impact. *Proc. 5th Int. Conf. on Erosion by Liquid and Solid Impact*, Paper 2. Cavendish Laboratory, Cambridge (1979).
[7] M. B. Lesser, Analytical solution of liquid drop impact problems. *Proc. Roy. Soc. Lond.* **A377**, 289–308 (1981).
[8] F. P. Bowden and J. H. Brunton, The deformation of solids by liquid impact at supersonic speeds. *Proc. Roy. Soc. Lond.* **A263**, 433–450 (1961).
[9] J. E. Field, D. A. Gorham, J. T. Hagan, M. J. Matthewson, M. V. Swain and S. van der Zwaag, Liquid jet impact and damage assessment for brittle solids. *Proc. 5th Int. Conf. on Erosion by Solid and Liquid Impact*, Paper 13. Cavendish Laboratory, Cambridge (1979).
[10] J. E. Field, D. A. Gorham and D. G. Rickerby, High speed liquid jet and drop impacts on brittle targets. *ASTM STP* 664 (Edited by W. F. Adler), pp. 298–319 (1979).
[11] S. M. Cherry, J. W. F. Goddard, M. P. M. Hall and G. R. Kennedy, Measurements of raindrop-size distributions using dual polarization radar. *Proc. 5th Int. Conf. on Erosion by Solid and Liquid Impact*, Paper 18. Cavendish laboratory, Cambridge (1979).
[12] J. Denis and D. Balgeas, Probabilistic evaluation of hydro-erosion hazards for missile radomes. *Proc. 5th Int. Conf. on Erosion by Liquid and Solid Impact*, Paper 19. Cavendish Laboratory, Cambridge (1979).
[13] D. A. Gorham and D. G. Rickerby, A hydraulic strength test for brittle samples. *J. Phys. E.* **8**, 794–796 (1975).
[14] M. J. Matthewson and J. E. Field, An improved strength measurement technique for brittle materials. *J. Phys. E.* **13**, 355–359 (1980).
[15] D. G. Rickerby, Ph.D. Thesis, University of Cambridge (1977).
[16] R. C. Shah and A. S. Kobayashi. ASTM Techn. Rep. 513 (1972).
[17] J. J. Mecholski, S. W. Freiman and R. W. Rice, Fracture surface analysis of ceramics. *J. Material Sci.* **11**, 1310–1319 (1976).
[18] M. M. Chaudhri and S. M. Walley, Damage to glass surfaces by the impact of small glass and steel spheres. *Phil. Mag. A.* **37**, 153–165 (1978).
[19] M. V. Swain and J. T. Hagan, Rayleigh wave interaction with and the extension of microcracks. *J. Material Sci.* **15**, 387–404 (1980).
[20] G. C. Sih, G. T. Embly and R. J. Ravera, Impact response of a finite crack in plane extension. *Int. J. Solids Structures* **8**, 977–993 (1972).
[21] L. B. Freund, Crack propagation in an elastic solid subjected to general loading—I. Constant rate of extension. *J. Mech. Phys. Solids* **20**, 129–140 (1972).
[22] L. B. Freund, Crack propagation in an elastic solid subjected to general loading—II Obliquely incident stress pulse. *J. Mech. Phys. Solids* **22**, 137–146 (1974).
[23] K. B. Broberg, The propagation of a brittle crack. *Ark. Phys.* **18**, 159–192 (1960).
[24] J. D. Eshelby, *Inelastic Behaviour of Solids* (Edited by M. F. Kanninen). McGraw-Hill, New York (1970).
[25] J. D. Achenbach and R. Neisumer, Fracture generated by a dilatational wave. *Int. J. Fracture Mech.* **7**, 77–88 (1971).
[26] L. F. R. Rose, Recent theoretical and experimental results on fast brittle fracture. *Int. J. Fracture Mech.* **12**, 799–813 (1976).
[27] S. Aoki, K. Kishimoto and M. Sakata, Dynamic problem of expanding cracks under concentrated load. *Engng Fract. Mech.* **11**, 301–314 (1979).
[28] K. Kishimoto, S. Aoki and M. Sakata, Computer simulation of a fast crack propagation in brittle materials. *Int. J. Fracture* **16**, 3–13 (1980).
[29] F. Kerkhoff and H. Richter, *Proc. 2nd Conf. on Fracture*, Brighton (1969).
[30] R. A. Hunt and L. N. McCartney, A new approach to Weibull's statistical theory of brittle fracture. *Int. J. Fracture* **15**, 365–375 (1979).
[31] A. De S. Jayatilaka and K. Trustrum, Statistical approach to brittle fracture. *J. Material Sci.* **12**, 1426–1430 (1977).
[32] D. G. Rickerby, Theoretical aspects of the statistical variation of strength. *J. Material Sci.* **15**, 2466–2470 (1980).
[33] M. J. Matthewson, Cavendish Lab., Cambridge. Private Communication.
[34] S. W. Wiederhorn and B. R. Lawn, Strength degradation of glass resulting from impacts with spheres. *J. Amer. Soc.* **60**, 451–458 (1977).

(*Received* 7 *December* 1981; *received for publication* 4 *February* 1982)